Experimental and kinetic modeling study of laminar coflow diffusion methane flames doped with 2-butanol

Hanfeng Jin [a], Wenhao Yuan [a], Yizun Wang [a], Yuyang Li [a], Fei Qi [a,b,*], Alberto Cuoci [c], Alessio Frassoldati [c], Tiziano Faravelli [c]

[a] *State Key Laboratory of Fire Science, University of Science and Technology of China, Hefei, Anhui 230026, PR China*
[b] *National Synchrotron Radiation Laboratory, University of Science and Technology of China, Hefei, Anhui 230029, PR China*
[c] *Department of Chemistry, Materials, and Chemical Engineering, Politecnico di Milano, Piazza Leonardo da Vinci 32, 20133 Milano, Italy*

Available online 25 June 2014

1. Introduction

Recognizing the challenges in energy sustainability and environmental security associated with the extensive use of fossil fuels, researchers have been redirecting their interests in biomass, in search of a suitable alternative of the fast depleting reserves of fossil fuels. As one of the four isomers of butanol, 2-butanol (sC_4H_9OH) can be produced from glucose through the bacterial fermentation and chemical conversion with high conversion efficiency [1]. Based on the investigation on the engine performance of 2-butanol/gasoline blends, 2-butanol was suggested as one

* Corresponding author at: National Synchrotron Radiation Laboratory, University of Science and Technology of China, Hefei, Anhui 230029, PR China. Fax: +86 551 65141078.
E-mail address: fqi@ustc.edu.cn (F. Qi).

of the potential gasoline surrogates for its favorable physical and chemical properties [2].

Compared with the comprehensive studies on *n*-butanol combustion, which are summarized in [3–6], 2-butanol is not under the spotlight. Some experimental studies have been performed on its combustion chemistry, including the measurements of global combustion parameters, like ignition delay times [7–9] and laminar burning velocities [10–12], and species profiles in flow reactor pyrolysis [13], shock tube pyrolysis [14], jet-stirred reactor oxidation [15], premixed flames [16,17] and coflow diffusion flames [18,19]. Meanwhile, Rosado-Reyes et al. [20] measured the unimolecular decomposition reaction rate constants of 2-butanol, which agreed satisfactorily with the calculations in [13]. Based on these experimental investigations, several kinetic models [4,5,13] have been developed, focusing on the initial fuel decomposition and oxidation process.

Alcohols are usually considered environmentally friendly due to the potential to reduce soot emission when doped in conventional transportation fuels. However, compared with hydrocarbon fuels with the same carbon number and similar molecular structure, they have a comparable sooting tendency [21]. In the premixed flames fueled with 2-butanol ($\phi = 1.70$) and *n*-butane ($\phi = 1.71$) under similar flame conditions [17,22], similar mole fractions of propargyl radical, cyclopentadiene and benzene were also observed, which implies the possible equivalent emission levels of PAHs in both flames. Meanwhile, in a comparative investigation of coflow diffusion methane flames doped with 2-butanol, *n*-butanol and *n*-butane [18,19], the benzene concentration was observed slightly higher in the methane/2-butanol flame than the other flames. Considering its future application as an additive of transportation fuels, it is important to better investigate the aromatic growth chemistry in the combustion of 2-butanol, especially when it interacts with hydrocarbon fuels.

Combined with the speciation using synchrotron vacuum ultraviolet photoionization mass spectrometry (SVUV-PIMS) [18] and the simulation using laminarSMOKE code [6,23], two laminar coflow diffusion methane flames doped with 2-butanol at atmospheric pressure were investigated in this work. Meanwhile, a kinetic model was developed from the recently reported kinetic models of butanols and aromatics [6,13,24], and validated against the experimental results. With the help of rate of production (ROP) analysis, interactions between 2-butanol and methane in the diffusion flame and main reaction pathways in the decomposition of 2-butanol and formation of aromatics were characterized in this work.

2. Experimental methods

The experiments were carried out at National Synchrotron Radiation Laboratory in Hefei, China. The beamlines and laminar coflow diffusion flame apparatus used in this work have been introduced in detail in previous studies [18,23]. In brief, the experimental apparatus consists of three parts, i.e. a coflow diffusion flame burner, a sampling system and a photoionization chamber with a reflectron time-of-flight mass spectrometer. The atmospheric pressure coflow flame was stabilized on a burner with a 10-mm-ID (inner diameter) stainless steel fuel tube located in the center of a 102-mm-ID air tube. Two flames were investigated in this work with different inlet mole fractions of 2-butanol in the fuel mixture (*Flame 1*: 3.90% sC_4H_9OH and 25.46% CH_4; *Flame 2*: 1.95% sC_4H_9OH and 33.27% CH_4) with the same inlet carbon flux. The gas phase flow rates of fuels (CH_4 and sC_4H_9OH), diluent gas (N_2), calibration gas (Ar) and air are presented in Table 1. The purities of CH_4, N_2, O_2, Ar and sC_4H_9OH are 99.995%, 99.999%, 99.999%, 99.99% and 99%, respectively. The mean velocities of fuel mixture and air were 13.34 and 16.55 cm/s in both flames, respectively. The gas flow rates were regulated by mass flow controllers, except for 2-butanol, which was injected into a vaporizer with its liquid flow rates regulated by a chromatography pump. In order to avoid the condensation of 2-butanol, the temperature of the vaporizer was kept at 30 K higher than its boiling point, and the temperature of the fuel mixture was kept at 493 K during the experiment.

Flame temperature profiles along the center line of the flames were measured with Pt-6%Rh/Pt-30%Rh thermocouple, which is 0.1 mm in diameter, and coated by Y_2O_3–BeO anticatalytic ceramic for the avoidance of catalytic effects. The uncertainty of the temperature measurement is about ±50 K. The gas temperature at the sooting region in the flame could be underestimated by about 120 K due to the soot condensation onto the thermocouples.

Table 1
Experimental conditions of coflow diffusion 2-butanol doped methane flames (Unit: SCCM).

Name	Q_{air}	Q_{Ar}	Q_{N_2}	Q_{CH_4}	$Q_{sC_4H_9OH}$
Flame 1	80,000	5.87	438	160	24.50
Flame 2	80,000	5.87	401	209	12.25

Note: Q_i is the flow rate of species *i*.

Flame species along the flame centerline were sampled, except in the region near the bottom of the flame, due to the shape limit of the sampling probe. The detailed flame sampling and data evaluation procedures were introduced in detail in [18]. The uncertainty of the experimental measurements is related to the probe sampling process and the photoionization cross sections (PICS) of flame species. The uncertainties of the measured mole fractions are within ±20% for flame species calculated with cold gas calibration, ±50% for stable flame species with well known PICSs, and about a factor of 2 for free radicals and the flame species with estimated PICSs [18,23]. The PICSs of flame species are available online in the database of [25].

3. Numerical simulation methods and kinetic models

The laminar coflow flames were numerically simulated with the laminarSMOKE code [6,23]. The detailed information for the design of the software was introduced elsewhere [26]. The radiation of the major flame species [27], Fickian and thermal diffusion [28] are taken into account. The transport properties of flame species are taken from the Chemkin transport database [29] or estimated following the procedure described in [30]. Because of the axial symmetry of the system, the numerical calculations were performed on a stretched, two-dimensional, rectangular domain, with length of 250 mm and width of 53 mm. Considering the balance between the accuracy of numerical calculation and the cost of computational time, a mesh with 5616 cells (156 × 36 cells) was found fine enough for the purpose of this work, also on the basis of previous studies [6]. Along the centerline, we adopted a finer numerical grid near the exit of the burner. Similarly, along the radial direction uniform cell spacing is adopted to describe the flame region, while coarser grid points are used in air flow. The fuel stream was assumed at 493 K with a parabolic velocity profile, while the coflow air was imposed at ambient temperature with a flat velocity profile. The composition of fuel mixture and the inlet boundary of air flow were fixed according to the data in Table 1.

A kinetic model was developed from the previously reported *n*-butanol model [6], and the sub-mechanism of 2-butanol was taken from the recently published 2-butanol model [13]. The aromatic formation sub-mechanism was improved based on our previous models [24], recent calculations [31–33] and other mechanisms [34–37], mainly including hydrogen-abstraction-carbon-addition (HACA) reactions [38] and the recombination reactions of resonant stabilized radicals with small flame species, like acetylene, propargyl and cyclopentadienyl radicals, etc. [24,34,35,37,39]. The thermodynamic properties of species in the present model are taken from different thermodynamic databases [40] or previous models [35]. This mechanism consists of 237 species and 1632 reactions (Provided in Supplemental Materials).

4. Results and discussion

Figure 1 shows the experimental and simulated mole fraction profiles of fuels (sC_4H_9OH and CH_4), O_2, major products (H_2, H_2O, CO, CO_2), dilution gas (N_2), and calibration gas (Ar) in the two flames. Figures 2 and 3 show the experimental and simulated mole fraction profiles of C2–C5 unsaturated intermediates and C6–C16 aromatic species in the two flames, respectively. By keeping constant carbon flux in the inlet fuel mixtures, the influence of 1.95% deviation in the inlet mole fraction of 2-butanol on the production of major products can be mostly eliminated, as illustrated from the almost invariable mole fraction profiles of major products (H_2, H_2O, CO, CO_2) in these two flames. In contrast, large influence on the production of many intermediates, especially benzene and other aromatic species, can be observed from Figs. 2 and 3.

4.1. Fuel decomposition

2-Butanol starts to decompose at around 1000 K at atmospheric pressure in flow reactor pyrolysis experiment [13]. Therefore, its decomposition process in the centerline of coflow flame can be divided into two stages. Taken *Flame 1* as an example, the gas temperature is 1000 K at around 20 mm above burner (HAB = 20 mm in Fig. 1a). In the low temperature region (HAB < 20 mm), weak H-abstraction reactions of 2-butanol occur via H-atom attack. The decrement of the mole fraction of 2-butanol in this region is due to the radial diffusion effect toward the flame front. A good agreement of the 2-butanol mole fractions in this region between the experimental and numerical results validates that the diffusion effect is well considered in the physical model. In the high temperature region (HAB > 20 mm), where most of 2-butanol is consumed, it dominantly decomposes via unimolecular decompositions.

Figure 4 shows the major reaction pathways in the decomposition of 2-butanol and the formation of the first aromatic ring in *Flame 1* based on the global ROP analysis along the flame centerline. As pointed out by Cai et al. [13] in their investigation on the pyrolysis of 2-butanol, unimolecular decomposition reactions are concluded as the dominant consumption channels of 2-butanol. Similarly, around 45% of 2-butanol decomposes through H_2O elimination reactions producing

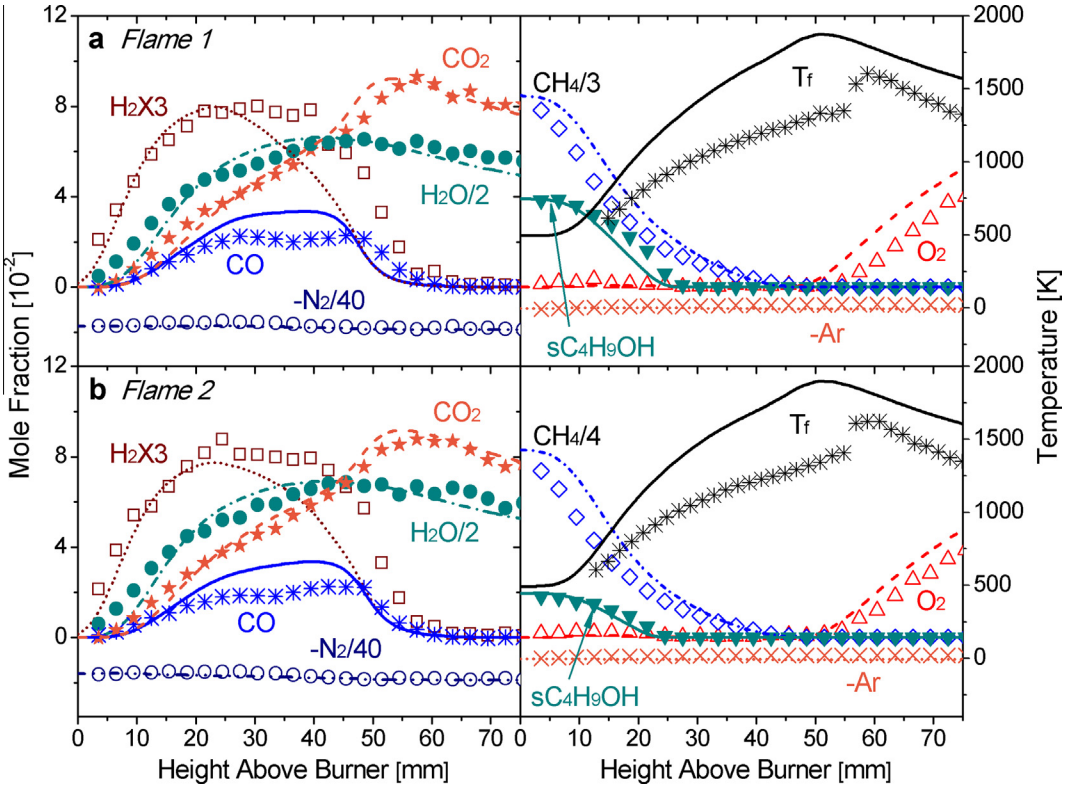

Fig. 1. Temperature and mole fractions of major flame species in the centerline of *Flame 1* (top) and *Flame 2* (bottom). Comparison between experimental measurements (symbols) and numerical simulations (lines).

1-butene and 2-butene under this flame condition. The further stepwise H-elimination reaction sequences of butene isomers can yield butadiene, vinylacetylene and butadiyne. Besides, around 30% of 2-butanol decomposes to ethyl and CH_3-CHOH radicals via another unimolecular decomposition channel. Due to the interaction between 2-butanol and methane in the high temperature region, the centerline of the coflow flame becomes an extreme pyrolysis environment. Since the ratio of 2-butanol/methane is only 0.06–0.15 in this experiment, the H-atom would dominantly react with methane due to the higher collision opportunity compared with 2-butanol. Local ROP analysis of H-atom in this region confirms that H-atom is mainly consumed via the reaction with methane, while it is produced via the decomposition of ethyl and CH_3CHOH radicals. Therefore, the unimolecular decomposition reactions dominate the consumption of 2-butanol in this region. The rate constants of the unimolecular reactions of 2-butanol in the present model was referred to the calculations of Cai et al. [13]. The good agreement between experimental measurements and model predictions of butene isomers (Fig. 2) provides a good validation of their calculations.

It can be also observed from Fig. 2 that the model can reasonably reproduce the mole fraction profiles of other primary decomposition products of 2-butanol. Ethylene is one of them, formed from the decomposition of ethyl radical. As shown in Fig. 4b, the unimolecular decomposition of 2-butanol only provides a minor part of ethyl radical, compared to the recombination of methyl radicals. In the coflow flames fueled with *n*-butanol/methane, unimolecular decomposition of *n*-butanol can produce ethylene via various intermediate radicals, including ethyl, C_2H_4OH and *n*-propyl radicals [41], while ethyl radical is the only ethylene precursor formed via the decomposition of 2-butanol at similar carbon bonds. Therefore, the position of OH group significantly affects the production ethylene from butanol isomers. Most of the yielded ethylene decomposes to acetylene. Another important acetylene formation pathway is the unimolecular decomposition of vinylacetylene, as shown in Fig. 4a.

Propene and allyl radical are the main decomposition products of butene isomers via the unimolecular decomposition or retro-ene reactions. Subsequently, allene is formed dominantly from allyl radical. The H-abstraction of allene is an additional propargyl formation pathway, which

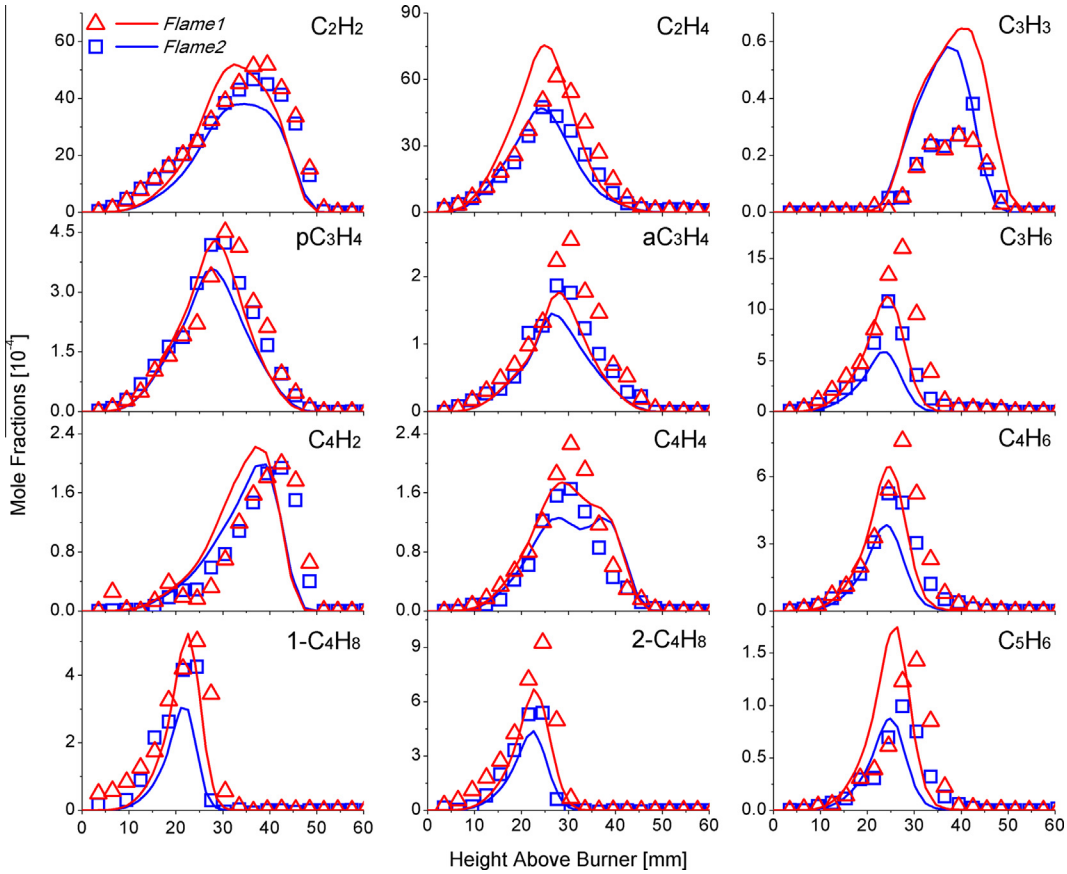

Fig. 2. Mole fraction comparison of C2–C5 intermediates between experimental data (symbols) and numerical predictions (lines), including acetylene (C_2H_2), ethylene (C_2H_4), propargyl radical (C_3H_3), propyne (pC_3H_4), allene (aC_3H_4), propene (C_3H_6), butadiyne (C_4H_2), vinylacetylene (C_4H_4), isomers of C_4H_6 (C_4H_6), 1-butene (1-C_4H_8), 2-butene (2-C_4H_8), and cyclopentadiene (C_5H_6).

is directly provided by the decomposition of 2-butanol. In contrast, propyne is formed through the reaction of acetylene and methyl radical ($H + pC_3H_4 = CH_3 + C_2H_2$, R1). The H-abstraction of propyne is the rate-controlling step in the formation of propargyl radical, which is consistent with the conclusions in our previous work on coflow diffusion flames of methane and methane/*n*-butanol [6,23]. As a result, propargyl radical, which is the dominant precursor of benzene under this flame condition, is mainly formed through the following reaction sequence: $CH_3 \rightarrow C_2H_5 \rightarrow C_2H_4 \rightarrow C_2H_3 \rightarrow C_2H_2 \rightarrow pC_3H_4 \rightarrow C_3H_3$. The addition of 2-butanol in methane flames enhances the formation of allene and acetylene, which subsequently increases the formation rate of propargyl radical and benzene. The present model can reproduce the peak positions and trends of the mole fraction profiles of propargyl radical. The discrepancies between the experimental and simulated maximum mole fractions can be mainly ascribed to the wall losses of free radicals in the sampling probe [42].

4.2. Formation of aromatic hydrocarbons

The recombination of allyl radical and acetylene plays a major role in the formation of cyclopentadiene (Fig. 2). It mainly decomposes to cyclopentadienyl radical, which is an important PAH precursor. With the increment of the doping ratio of 2-butanol in the flames, it increases the mole fractions of cyclopentadienyl radical, which enhances the contributions of C5 pathways in the formation of aromatic species.

As shown in Fig. 4b, around 40% of benzene in *Flame 1* is formed through reaction $C_3H_3 + C_3H_3 = C_6H_6$ (R2), and the recombination of propargyl radical with propyne and allene plays an additional role. Phenyl radical is also formed from propargyl radical via $C_3H_3 + C_3H_3 = C_6H_5 + H$ (R3), which was concluded as the most sensitive reaction in our previous modeling study on methane coflow flames [6]. The H-abstraction reaction of benzene is another important formation channel, because of the large production of benzene in the flames. Model predictions of benzene and

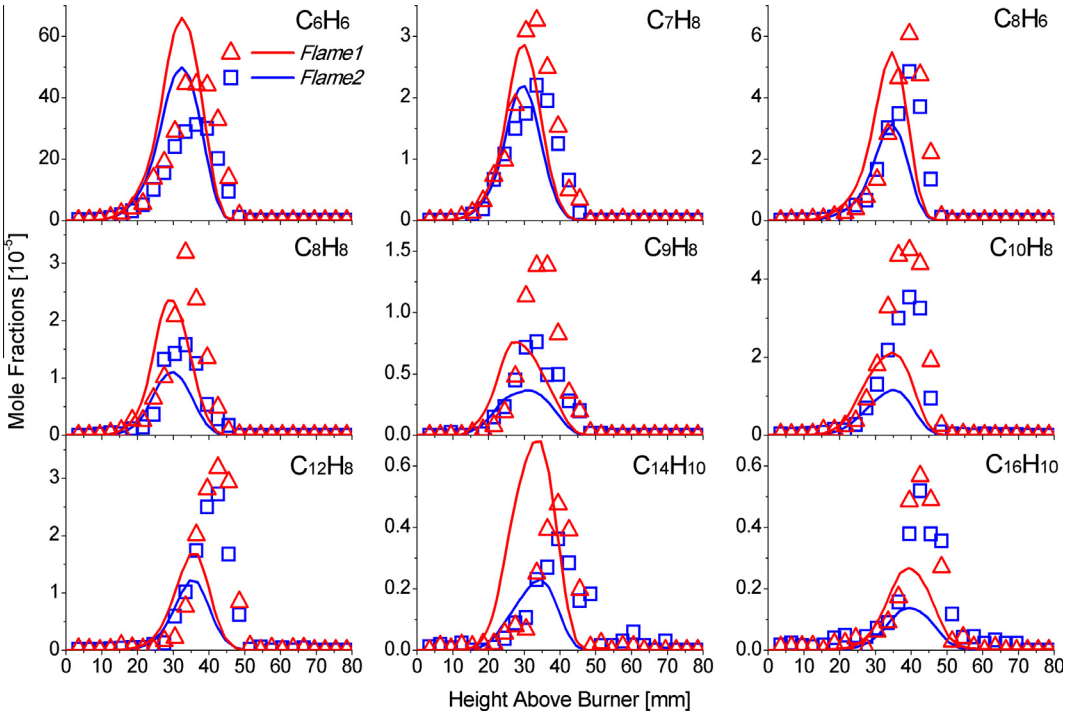

Fig. 3. Mole fraction comparison of C6–C16 aromatic species between experimental data (symbols) and numerical predictions (lines), including benzene (C_6H_6), toluene (C_7H_8), phenylacetylene (C_8H_6), styrene (C_8H_8), indene (C_9H_8), naphthalene ($C_{10}H_8$), acenaphthalene and ethynylnaphthalene ($C_{12}H_8$), phenanthrene and anthracene ($C_{14}H_{10}$), and pyrene and fluoranthene ($C_{16}H_{10}$).

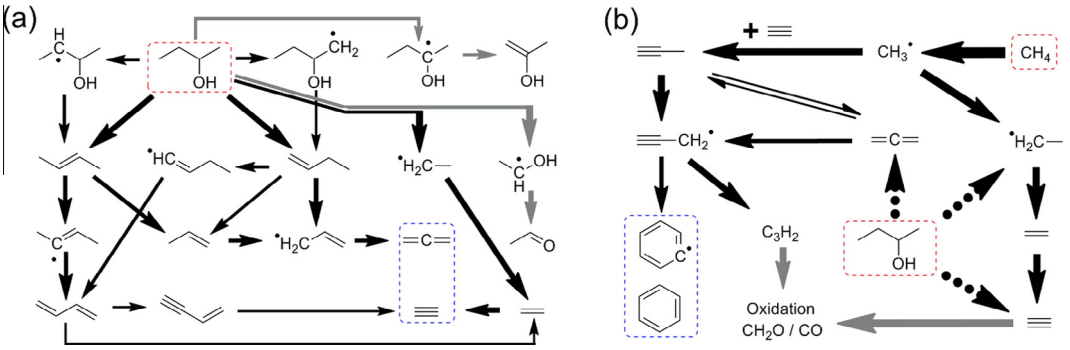

Fig. 4. (a) Major decomposition pathways of 2-butanol; (b) major reaction pathways in the formation of the first aromatic ring in *Flame 1*. The thickness of the arrow is proportional to the carbon flux of the pathway. The oxidation reactions are highlighted with gray arrows. The dotted arrows in (b) denote the simplified process in (a).

other observed monocyclic aromatic hydrocarbons (MAHs) including toluene, styrene and phenylacetylene, are presented in Fig. 3. The reactions between benzene/methyl radical, phenyl/ethylene and phenyl/acetylene are their main formation pathways, respectively. Benzyl radical, that is mainly formed from toluene and phenyl radical ($C_6H_5 + CH_3 = C_6H_5CH_2 + H$, R4), is one of the key PAH precursors to be discussed in the following paragraphs. Based on the ROP analysis along the flame centerline, the major reaction pathways in the formation of PAHs in *Flame 1* are drawn in Fig. 5.

Indene and naphthalene are two important bicyclic PAHs, and their formation represents the starting point of PAH formation. Their model predictions are presented in the middle row of Fig. 3. According to the pathway analysis in

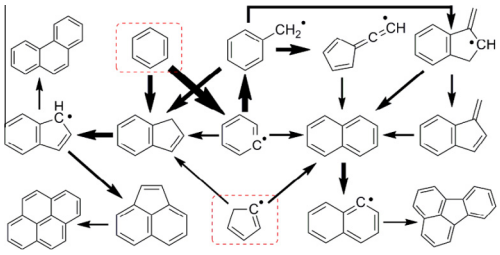

Fig. 5. Major reaction pathways in the formation of large aromatic species in *Flame 1*. The thickness of the arrow is proportional to the carbon flux of the pathway.

Fig. 5, the reaction between benzyl radical/acetylene ($C_6H_5CH_2 + C_2H_2 = C_9H_8 + H$, R5) dominates the formation of indene. The rate constant of R5 adopted in the present model was estimated by Blanquart et al. [35], which agreed well with the calculation of Vereecken and Peeters [43]. With the increasing of the doping ratio of 2-butanol, it enhances the contribution of R5 (up to 40% in *Flame 1*) due to the increment of benzyl radical and acetylene in flames. Meanwhile, the reaction between benzene/propargyl radical ($C_6H_6 + C_3H_3 = C_9H_8 + H$, R6) proposed by Li et al. [24], phenyl radical/propyne ($C_6H_5 + pC_3H_4 = C_9H_8 + H$, R7) and phenyl radical/allene ($C_6H_5 + aC_3H_4 = C_9H_8 + H$, R8) calculated by Kaiser et al. [44] play an additional role with an overall contribution around 30% in *Flame 1*.

As shown in Fig. 5, naphthalene is mainly formed through five pathways, all of which are the combination reactions of resonantly stabilized free radicals with small species. By doping 2-butanol into the flames, it increases the mole fractions of benzyl, phenyl, and cyclopentadienyl radicals, which leads to a larger production of naphthalene. In the present model, the reaction steps of benzyl and propargyl radicals were referred to the calculation of Matsugi and Miyoshi [36], replacing the global reaction $C_6H_5CH_2 + C_3H_3 = C_{10}H_8 + 2H$ (R9) in our previous models [6,24]. The intermediate species methyleneindanyl ($C_9H_7CH_2$) radical is primarily formed through $C_6H_5CH_2 + C_3H_3 = C_9H_7CH_2 + H$ (R10). And then, naphthalene is yielded from the following isomerization and H-elimination of methyleneindanyl through $C_9H_7CH_2(+M) = C_{10}H_8 + H(+M)$ (R11). Methyleneindene that formed via another channel of the H-elimination of methyleneindanyl radical, can isomerize to naphthalene through $C_9H_6CH_2 + H = C_{10}H_8 + H$ (R12). The rates of these reactions provided in Chembyshev format in [32] were refitted into Arrhenius format here. The rate of R10 was estimated as the rate of the global reaction R9 recommended by Richter and Howard [34]. There is another efficient pathway from benzyl radical, via the intermediate of fulvenallene (C_7H_6) and fulvenallyl (C_7H_5) radical: benzyl → fulvenallene → fulvenallyl → naphthalene. The decomposition kinetics of benzyl radical was referred to the proposition of Derudi et al. [31], which would yield fulvenallyl (C_7H_5) during the process. Its reaction with propargyl radical ($C_7H_5 + C_3H_3 = C_{10}H_8$, R13) forming naphthalene was proposed similar to the combination of propargyl radical forming benzene. Compared to the contribution of the former pathways (around 10%), it provides a contribution of 40% in global naphthalene formation in *Flame 1*. Naphthalene can be also formed via the reactions between phenyl and C4 species. Among them, the reaction of phenyl radical/vinylacetylene ($C_6H_5 + C_4H_4 = C_{10}H_8 + H$, R14) is an efficient pathway, which was suggested in the works of Richter and Howard [34] and Blanquart et al. [35]. Similar to the proposition in the previous models [34–37] and the observation in coflow flames [6,23], the self-combination of cyclopentadienyl radical is also an additional naphthalene formation pathway under this flame condition.

Acenaphthylene ($C_{12}H_8$), phenanthrene ($pC_{14}H_{10}$), anthracene, pyrene and fluoranthene ($fC_{16}H_{10}$) are important tricyclic and tetracyclic PAHs. As shown in Fig. 5, reaction $C_9H_7 + C_3H_3 = C_{12}H_8 + 2H$ (R15) proposed in the former studies of Slavinskaya et al. [37] and is the dominant formation pathway of acenaphthylene in the present model. Phenanthrene is mainly formed through the combination of indenyl and cyclopentadienyl radicals ($C_9H_7 + C_5H_5 = pC_{14}H_{10} + 2H$, R16). The rate of R16 recommended in the work of Blanquart et al. [35] was adopted in present model, which was close to the estimation of Cavallotti et al. [33] and Richter and Howard [34]. Pyrene was mainly formed through the reaction between acenaphthylenyl radical and butadiyne, which was proposed by Slavinskaya et al. [37]. Fluoranthene, that is the isomer of pyrene, was dominantly formed through the combination of naphthyl and phenyl radicals ($C_{10}H_7 + C_6H_5 = fC_{16}H_{10} + 2H$, R17). The rate constant of this reaction was estimated from the recombination of phenyl radical calculated by Park and Lin [45]. The experimental measured and simulated mole fractions of these PAHs are shown in the last row of Fig. 3. The present model captures the effect of the doping of 2-butanol very well, however, does not predict the peak values of their mole fractions properly.

5. Conclusions

In this work, two coflow methane flames doped with 2-butanol were studied with SVUV-PIMS. A 2-butanol kinetic model extended to aromatic growth mechanism was developed, giving a better characterization on the benzene and PAH formation. Numerical simulations with detailed kinetic

mechanism were performed with laminarSMOKE. The interaction between 2-butanol and methane in the aromatic formation process was analyzed in detail. The impact of the doping of 2-butanol is found to be pronounced for benzene formation by increasing the mole fractions of C2 and C3 species, which subsequently lead to the increment of propargyl radical.

Resonance stabilized free radicals, such as cyclopentadienyl, phenyl, and benzyl radicals are main PAH precursors, or even indenyl and naphthyl radicals for large PAHs. And the reactions of these radicals with small hydrocarbon intermediates (C2–C4 species) or themselves are the most efficient aromatic grown pathways. Considering the balance of the reactivity and the residence time of the intermediate species in the flames, resonant stabilized free radicals, which are more active than stable intermediates in chemical reactions and have longer residence time than active free radicals, should have much more opportunity to be involved in the PAH formation procedure. Further theoretical investigation and accurate experimental measurements on the growth of large PAH species are demanded to reproduce their formation accurately under a wide range of combustion conditions.

Acknowledgements

Authors are grateful for funding supports from National Basic Research Program of China (973 Program) (2013CB834602), Natural Science Foundation of China (51127002), Chinese Universities Scientific Fund (WK2320000020) and Chinese Academy of Sciences.

Appendix A. Supplementary material

Supplementary data associated with this article can be found, in the online version.

References

[1] P.S. Nigam, A. Singh, *Prog. Energy Combust. Sci.* 37 (2011) 52–68.
[2] E. Christensen, J. Yanowitz, M. Ratcliff, R.L. McCormick, *Energy Fuels* 25 (2011) 4723–4733.
[3] J. Cai, L. Zhang, F. Zhang, Z. Wang, Z. Cheng, W. Yuan, F. Qi, *Energy Fuels* 26 (2012) 5550–5568.
[4] A. Frassoldati, R. Grana, T. Faravelli, E. Ranzi, P. Oßwald, K. Kohse-Höinghaus, *Combust. Flame* 159 (2012) 2295–2311.
[5] S.M. Sarathy, S. Vranckx, K. Yasunaga, M. Mehl, P. Oßwald, W.K. Metcalfe, C.K. Westbrook, W.J. Pitz, K. Kohse-Höinghaus, R.X. Fernandes, H.J. Curran, *Combust. Flame* 159 (2012) 2028–2055.
[6] H.F. Jin, A. Cuoci, A. Frassoldati, T. Faravelli, Y.Z. Wang, Y.Y. Li, F. Qi, *Combust. Flame* 161 (2014) 657–670.
[7] J.T. Moss, A.M. Berkowitz, M.A. Oehlschlaeger, J. Biet, V. Warth, P.A. Glaude, F. Battin-Leclerc, *J. Phys. Chem. A* 112 (2008) 10843–10855.
[8] K. Yasunaga, T. Mikajiri, S.M. Sarathy, T. Koike, F. Gillespie, T. Nagy, J.M. Simmie, H.J. Curran, *Combust. Flame* 159 (2012) 2009–2027.
[9] I. Stranic, D.P. Chase, J.T. Harmon, S. Yang, D.F. Davidson, R.K. Hanson, *Combust. Flame* 159 (2012) 516–527.
[10] P.S. Veloo, F.N. Egolfopoulos, *Proc. Combust. Inst.* 33 (2011) 987–993.
[11] X. Gu, Z. Huang, S. Wu, Q. Li, *Combust. Flame* 157 (2010) 2318–2325.
[12] F. Wu, C.K. Law, *Combust. Flame* 160 (2013) 2744–2756.
[13] J. Cai, W. Yuan, L. Ye, Z. Cheng, Y. Wang, L. Zhang, F. Zhang, Y. Li, F. Qi, *Combust. Flame* 160 (2013) 1939–1957.
[14] I. Stranic, S.H. Pyun, D.F. Davidson, R.K. Hanson, *Combust. Flame* 160 (2013) 1012–1019.
[15] C. Togbé, A. Mze-Ahmed, P. Dagaut, *Energy Fuels* 24 (2010) 5244–5256.
[16] B. Yang, P. Oßwald, Y. Li, J. Wang, L. Wei, Z. Tian, F. Qi, K. Kohse-Höinghaus, *Combust. Flame* 148 (2007) 198–209.
[17] P. Oßwald, H. Güldenberg, K. Kohse-Höinghaus, B. Yang, T. Yuan, F. Qi, *Combust. Flame* 158 (2011) 2–15.
[18] H. Jin, Y. Wang, K. Zhang, H. Guo, F. Qi, *Proc. Combust. Inst.* 34 (2013) 779–786.
[19] C.S. McEnally, L.D. Pfefferle, *Proc. Combust. Inst.* 30 (2005) 1363–1370.
[20] C.M. Rosado-Reyes, W. Tsang, *J. Phys. Chem. A* 116 (2012) 9599–9606.
[21] C.S. McEnally, L.D. Pfefferle, *Environ. Sci. Technol.* 45 (2011) 2498–2503.
[22] P. Oßwald, K. Kohse-Höinghaus, U. Struckmeier, T. Zeuch, L. Seidel, L. Leon, F. Mauss, Z. Physik, *Chemie* 225 (2011) 1029–1054.
[23] A. Cuoci, A. Frassoldati, T. Faravelli, H. Jin, Y. Wang, K. Zhang, P. Glarborg, F. Qi, *Proc. Combust. Inst.* 34 (2013) 1811–1818.
[24] Y. Li, J. Cai, L. Zhang, T. Yuan, K. Zhang, F. Qi, *Proc. Combust. Inst.* 33 (2011) 593–600.
[25] Photonionization Cross Section Database (Version 1.0), National Synchrotron Radiation Laboratory, Hefei, China, 2011. <http://www.flame.nsrl.ustc.edu.cn/en/database.htm>.
[26] A. Cuoci, A. Frassoldati, T. Faravelli, E. Ranzi, *Combust. Flame* 160 (2013) 870–886.
[27] R.J. Hall, *J. Quant. Spectrosc. Radiat. Transfer* 49 (1993) 517–523.
[28] S. Chapman, T.G. Cowling, *The mathematical Theory of Non-Uniform Gases*, Cambridge University Press, Cambridge, 1970.
[29] R.J. Kee, J. Warnatz, J.A. Miller, *Chemkin II: A Fortran Chemical Kinetics Package for the Evaluation of Gas-Phase Viscosities, Conductivities and Diffusion Coefficient*, Sandia National Laboratory, 1983.
[30] H. Wang, M. Frenklach, *Combust. Flame* 96 (1994) 163–170.
[31] M. Derudi, D. Polino, C. Cavallotti, *Phys. Chem. Chem. Phys.* 13 (2011) 21308–21318.

[32] A. Matsugi, A. Miyoshi, *Int. J. Chem. Kinet.* 44 (2012) 206–218.
[33] C. Cavallotti, D. Polino, A. Frassoldati, E. Ranzi, J. *Phys. Chem. A* 116 (2012) 3313–3324.
[34] H. Richter, J.B. Howard, *Phys. Chem. Chem. Phys.* 4 (2002) 2038–2055.
[35] G. Blanquart, P. Pepiot-Desjardins, H. Pitsch, *Combust. Flame* 156 (2009) 588–607.
[36] A. Matsugi, A. Miyoshi, *Proc. Combust. Inst.* 34 (2013) 269–277.
[37] N.A. Slavinskaya, U. Riedel, S.B. Dworkin, M.J. Thomson, *Combust. Flame* 159 (2012) 979–995.
[38] H. Wang, M. Frenklach, *Combust. Flame* 110 (1997) 173–221.
[39] A. D'Anna, J.H. Kent, *Combust. Flame* 132 (2003) 715–722.
[40] E. Goos, A. Burcat, B. Ruscic, Ideal Gas Thermochemical Database with Updates from Active Thermochemical Table, 2005. <ftp://ftp.technion.ac.il/pub/supported/aetdd/thermodunamics>.
[41] H.F. Jin, A. Cuoci, A. Frassoldati, T. Faravelli, Y.Z. Wang, Y.Y. Li, F. Qi, *Combust. Flame* 161 (2014) 657–670.
[42] C.S. McEnally, L.D. Pfefferle, B. Atakan, K. Kohse-Hoinghaus, *Prog. Energy Combust. Sci.* 32 (2006) 247–294.
[43] L. Vereecken, J. Peeters, *Phys. Chem. Chem. Phys.* 5 (2003) 2807–2817.
[44] R.I. Kaiser, L. Vereecken, J. Peeters, H.F. Bettinger, P.R. Schleyer, H.F. SchaeferIII, *Astron. Astrophys.* 406 (2003) 385–391.
[45] J. Park, M.C. Lin, *J. Phys. Chem. A* 101 (1997) 14–18.